

## Article

# Electroextraction of Ytterbium on the Liquid Lead Cathode in LiCl-KCl Eutectic

Zhuyao Li <sup>1,2</sup> , Liandi Zhu <sup>2</sup>, Dandan Tang <sup>1,\*</sup>, Ying Dai <sup>2</sup>, Feiqiang He <sup>2</sup>, Zhi Gao <sup>2</sup>, Cheng Liu <sup>2</sup>, Hui Liu <sup>2</sup>, Limin Zhou <sup>2</sup>, Zhirong Liu <sup>1,2</sup> and Jinbo Ouyang <sup>2,\*</sup>

<sup>1</sup> State Key Laboratory of Nuclear Resources and Environment, East China University of Technology, Nanchang 330013, China

<sup>2</sup> School of Chemistry, Biological and Materials Sciences, East China University of Technology, Nanchang 330013, China

\* Correspondence: tangdandan@ecut.edu.cn (D.T.); ouyangjinbo@ecut.edu.cn (J.O.)

**Abstract:** The reduction mechanisms of Yb(III) on W electrodes in molten LiCl-KCl-YbCl<sub>3</sub> were explored at 773 K, and the diffusion coefficient of Yb(III) was determined. Then, various electrochemical techniques were employed to investigate the electroreduction of Yb(III) in molten LiCl-KCl on a liquid Pb film and Pb electrode. Electrochemical signals were associated with forming Pb<sub>3</sub>Yb, PbYb, Pb<sub>3</sub>Yb<sub>5</sub>, and PbYb<sub>2</sub>. The deposition potentials and equilibrium potentials of four Pb-Yb intermetallics were obtained through open-circuit chronopotentiometry. Metallic Yb was extracted by potentiostatic electrolysis (PE) on a liquid Pb electrode, and XRD analyzed the Pb-Yb alloy obtained at different extraction times. The recovered Yb was found in the form of Pb<sub>3</sub>Yb and PbYb intermetallics. The extraction efficiency of Yb was calculated according to ICP analysis results, and extraction effectivity could attain 94.5% via PE at −1.86 V for 14 h.

**Keywords:** electrochemical extraction; ytterbium; liquid Pb electrode; Pb-Yb alloy; electrochemical behavior



**Citation:** Li, Z.; Zhu, L.; Tang, D.; Dai, Y.; He, F.; Gao, Z.; Liu, C.; Liu, H.; Zhou, L.; Liu, Z.; et al.

Electroextraction of Ytterbium on the Liquid Lead Cathode in LiCl-KCl Eutectic. *Crystals* **2022**, *12*, 1453. <https://doi.org/10.3390/cryst12101453>

Academic Editor: Stefano Carli

Received: 15 September 2022

Accepted: 11 October 2022

Published: 14 October 2022

**Publisher's Note:** MDPI stays neutral with regard to jurisdictional claims in published maps and institutional affiliations.



**Copyright:** © 2022 by the authors. Licensee MDPI, Basel, Switzerland. This article is an open access article distributed under the terms and conditions of the Creative Commons Attribution (CC BY) license (<https://creativecommons.org/licenses/by/4.0/>).

## 1. Introduction

The increasing demand of human beings for energy and the promotion of global low-carbon energy has increased the number of nuclear power stations in the world [1,2]. However, the management, storage, and disposal of used nuclear fuel (UNF) discharged from nuclear power plants has become a worldwide issue [3,4]. A 1000 MWe nuclear reactor generates about 25–30 tons of UNF annually [5,6]. Based on the International Atomic Energy Agency (IAEA) estimate, around 450 operating nuclear power plants have generated a global inventory of some 270,000 metric tons of UNF [7,8]. Pyroprocessing is one of the most promising technologies for treating UNF, and electrorefining is an essential unit operation in the pyroprocessing technique [9–12].

In electrorefining of UNF in molten LiCl-KCl, the standard potentials of lanthanide elements (Lns) are more negative than those of actinide elements (Ans) [13–15]. U and transuranic elements (TRUs) are deposited onto the cathode, and various lanthanide fission products contained in UNF dissolve in the molten salt. During the electrolysis process, Lns accumulate, which makes difficult the separation of Ans and Lns [16–23]. Therefore, proper electrode materials have a good effect on the separation process of Ans and Lns. Compared with the solid cathode, the liquid metal cathode has been widely studied because of its constant surface area and easy diffusion of deposits to liquid metal. Jiao et al. [24] summarized liquid metals from the aspects of properties, depolarization effects, alloy preparation, etc., such as liquid Bi [25–28], Pb [29–32], Sn [33–36], and Ga [37–40], which provided a reference for molten salt electrorefining.

In addition, lead has a low melting point (327 °C), and through evaluating the vapor pressures of various liquid metals, we discovered that the order of separating Ans and Lns from the liquid metal cathode via distillation is: Cd > Zn > Pb > Bi > Al > Ga > Sn. Liquid

Pb appears to be a proper candidate for electrode material in separating and extracting Ans and Lns from molten salt by electrowinning. After electrowinning, a Pb-Ans/Lns alloy can be formed on the liquid Pb electrode. Finally, the cathode deposits can be separated from the liquid Pb cathode by Pb distillation. Therefore, lead was employed as the cathode for ytterbium extraction in this work. In our previous work, liquid lead was used as a cathode due to the underpotential deposition of Dy(III) on the liquid Pb electrode. The reduction potential of Dy on the liquid Pb electrode is  $-1.35$  V (vs. Ag/AgCl), which is more positive than that on the W electrode. Dysprosium was extracted from molten LiCl-KCl-DyCl<sub>3</sub>, and the extraction efficiency of dysprosium reached 97.2% [41,42]. Ytterbium is a variable valence element, one of the typical rare earth fission elements. Ji et al. [43] studied the electrochemical properties of ytterbium on liquid Zn electrodes in LiCl-KCl melts. Li et al. [44] studied the electrochemical behavior of Yb(III) on Cu electrodes in LiCl-KCl melts. Yan et al. [45] researched ytterbium and zinc co-deposition in LiCl-KCl-ZnCl<sub>2</sub>-YbCl<sub>3</sub> melts on a W electrode. However, there is little information about the extraction of ytterbium from molten chlorides on liquid lead cathodes.

In the present study, different electrochemical techniques were used to explore the reduction mechanisms of Yb(III) on W, liquid Pb film, and liquid Pb electrodes. Moreover, the recovery of Yb from molten salt was executed by PE, and the products were characterized by SEM-EDS and XRD.

## 2. Experimental

All electrochemical measurements were carried out in an alumina crucible with LiCl-KCl (55.8 wt%) melts in an electric furnace. Yb was introduced into the LiCl-KCl melts as dehydrated YbCl<sub>3</sub> powder (analytical grade). The reference electrode consisted of a silver wire (1 mm in diameter) immersed in a 1.5 wt% AgCl solution. A spectral pure graphite rod (6 mm in diameter) was used as a counter electrode. A tungsten wire (1 mm in diameter, 99.95%), a Pb film electrode (Pb coated on a W wire), and liquid lead (99%) were used for the working electrodes. PE and electrochemical measurements were performed (Metrohm, Ltd., Autolab PGSTAT 302N with Nova 1.10 software). The resistance between the reference electrode and the working electrode in molten salt was calculated by electrochemical impedance spectroscopy (EIS). The EIS was performed under the open circuit potential of the LiCl-KCl molten salt system under the condition of 10 mV amplitude over a 0.01-10000 Hz frequency range, as shown in Figure 1. According to Figure 1, the solution resistance ( $R_s$ ) of the molten LiCl-KCl was  $0.62 \Omega$  determined at 773 K. After the ohmic potential (IR) compensation, cyclic voltammograms (CVs) were obtained. The phase composition of extraction products was characterized using XRD (Philips, Amsterdam, The Netherlands). The metal ion concentration in the melts was analyzed by ICP-AES (USA Thermo Elemental, IRIS Intrepid II XSP). Figure 2 shows the schematic setup of three-electrode electrochemical cells inside the furnace.

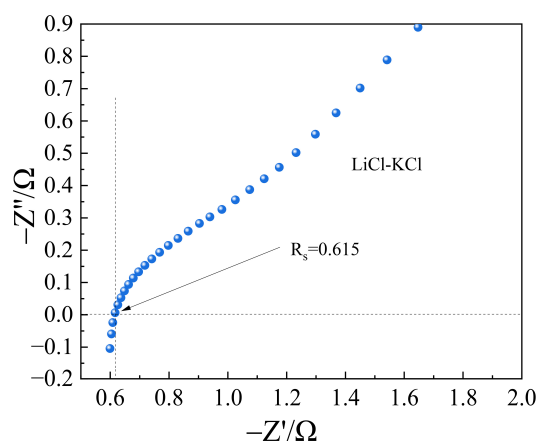


**Figure 1.** EIS data on the W electrode in molten LiCl-KCl at temperatures of 773 K.

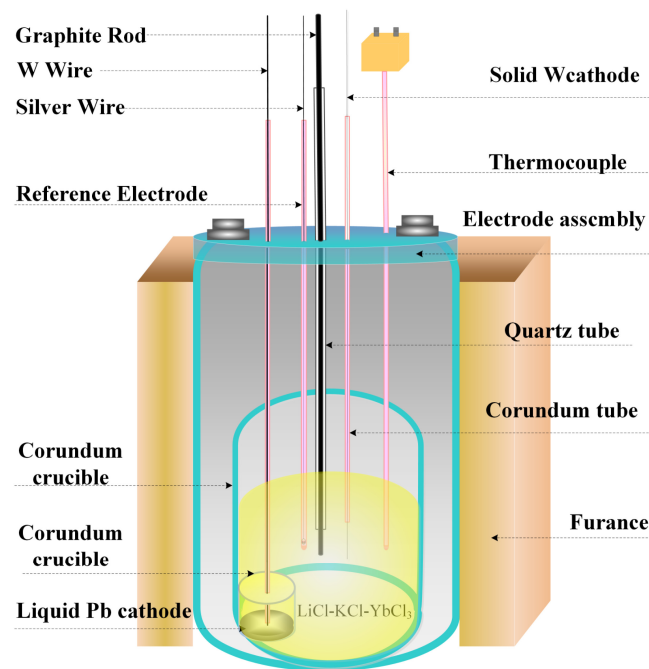


**Figure 2.** The schematic setup of three-electrode electrochemical cells inside the furnace.

### 3. Results and Discussion

#### 3.1. Electrode Reaction of Yb(III) on the W Electrode

Figure 3 shows the CVs attained in LiCl-KCl and LiCl-KCl-YbCl<sub>3</sub> melts on the W electrode. The redox couples R<sub>A</sub>/O<sub>A</sub> (−2.39/−2.28 V) are considered as the redox of Li(I)/Li(0) on the W electrode. When YbCl<sub>3</sub> is added, the newly added electrochemical signal R<sub>B</sub>/O<sub>B</sub> (−0.47/−0.32 V) corresponds to Yb(III)/Yb(II). No electrochemical signal of Yb(II) reduction to Yb was found, which indicates that the reduction potential of Yb(II) is more negative than that of Li (I) [43,44]. In this system, Yb(III) first becomes a low valence ion and is then oxidized to a high valence state. No metal Yb was obtained on the W electrode. They are thought to correspond to the following reaction.

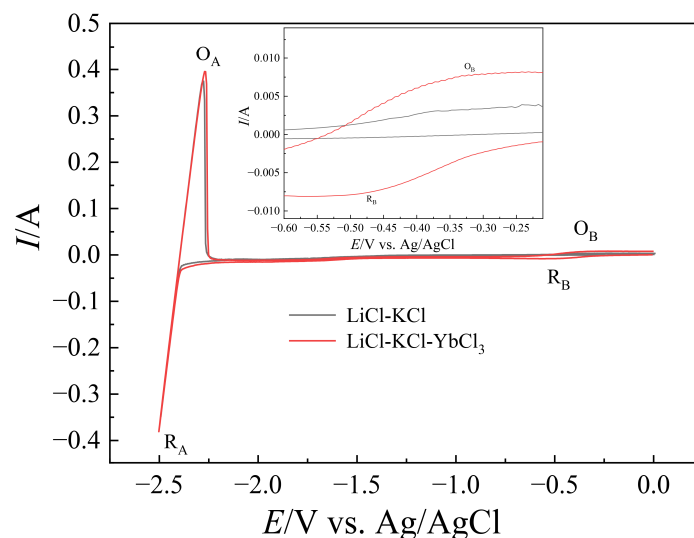


**Figure 3.** CVs obtained on the W electrode ( $S = 0.314 \text{ cm}^2$ ) in the absence and presence of YbCl<sub>3</sub> ( $1.55 \times 10^{-4} \text{ mol cm}^{-3}$ ) in eutectic LiCl-KCl.

Typical CVs of molten LiCl-KCl-YbCl<sub>3</sub> recorded on the W electrodes at various scan rates are shown in Figure 4a. What can be observed is that with an increase in scan rate, the peak potential for R<sub>B</sub> was constant (Figure 4b). Therefore, it can be decided that the electrode reduction reaction R<sub>B</sub> is a reversible process on scan rate in a range of 0.08–0.28 V s<sup>-1</sup>. Figure 4b illustrates the linear relationship of  $I_p$  and  $v^{-1/2}$  of Yb(III) in molten LiCl-KCl-YbCl<sub>3</sub>, indicating that the redox reaction is controlled by diffusion. In a soluble/soluble system, for the chemical reaction controlled by the mass transfer rate step, there is a relationship between the cathode peak current and the square root of the sweep rate, which can be described by Randles–Sevcik equation as follows [43]:

$$I_p = 0.4463(nF)^{3/2}(RT)^{-1/2}SCD^{1/2}v^{1/2} \quad (2)$$

where  $S$  represents the surface area of the working electrode,  $C_0$  represents the bulk concentration of the Yb(III) ion,  $D$  corresponds to the diffusion coefficient,  $I$  corresponds to the applied current,  $n$  corresponds to the number of exchanged electrons,  $F$  corresponds to the Faraday constant, and  $v$  represents the potential scan rate.

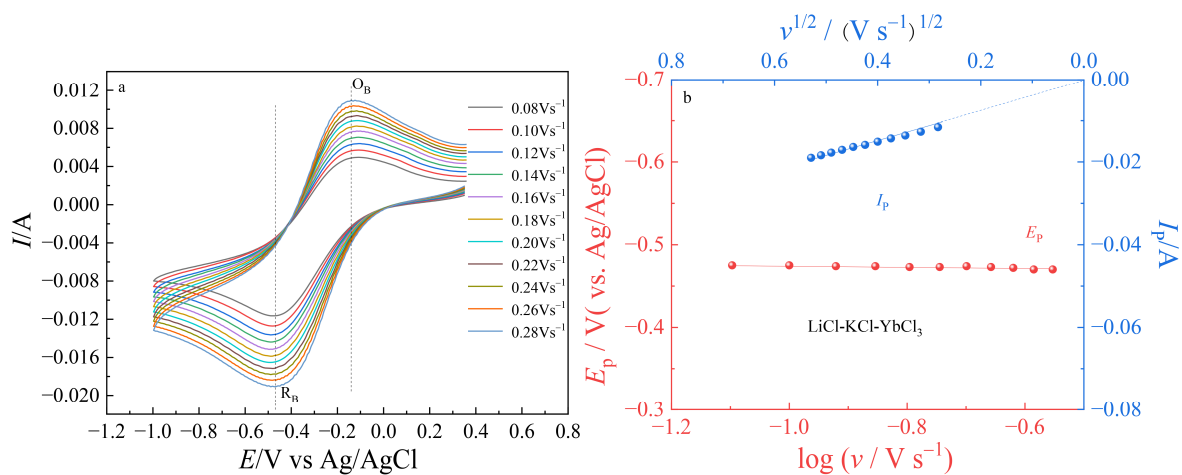


**Figure 4.** (a) CVs obtained on the W electrode at different scan rates in molten LiCl-KCl-YbCl<sub>3</sub>; (b) peak potential of the cathodic R<sub>B</sub> vs.  $\log v$  derived from (a); peak current of the cathodic R<sub>B</sub> vs. the square root of scan rate derived from (a).

The calculated diffusion coefficient of Yb(III) at 773 K was  $1.86 \times 10^{-5} \text{ cm}^2 \text{ s}^{-1}$ . The diffusion coefficient of the Yb(III) ion in LiCl KCl molten salt calculated by Smolenski et al. at 848 K is  $2.7 \times 10^{-5} \text{ cm}^2 \text{ s}^{-1}$ , which is consistent with our research results [46].

Square wave voltammetry (SWV) was carried out to measure the number of electrons transferred during the reduction process of Yb(III) on the W electrode.

Figure 5a depicts the SWV curves gained in LiCl-KCl-YbCl<sub>3</sub> molten salt at different frequencies. One reduction signal, R<sub>B</sub> (−0.47 V), correlated with the reduction process of Yb(III) to Yb(II). Furthermore, the shape of R<sub>B</sub> was flat and symmetrical, which indicates that the electrode reactions were reversible in a soluble/soluble system. The linear relationship between  $I_{pc}$  and  $f^{1/2}$  suggests that the reduction of Yb(III) on the W electrode was controlled by diffusion. Therefore, the number of electrons transferred was calculated from  $W_{1/2}$  using Equation (3) [42]:

$$W_{1/2} = 3.52 \frac{RT}{nF} \quad (3)$$

where  $W_{1/2}$  is the half-peak width of the SWV curve, and the calculated number of electrons transferred from the reduction of Yb(III) to Yb(II) is close to 1 (Table 1).

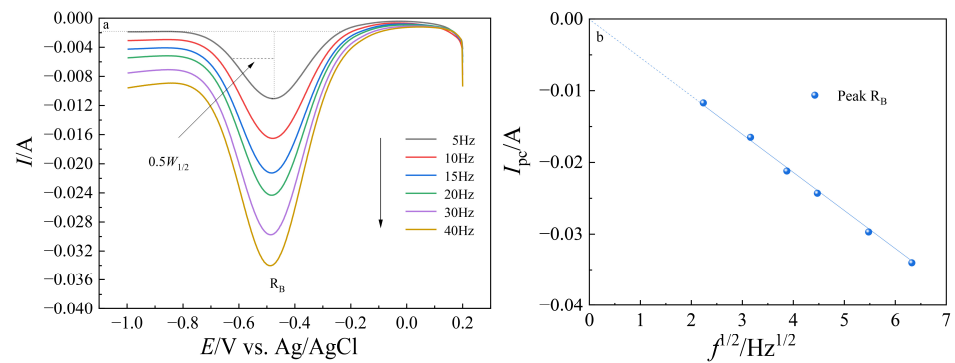


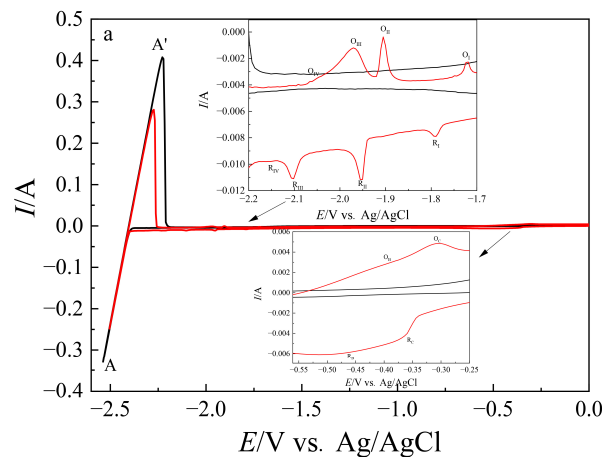
**Figure 5.** (a) SWV curves for the reduction of Yb(III) on the W electrode at 773 K; pulse height: 100 mV; step potential: 5 mV; frequency: 5–40 Hz. (b) The linear relationship of  $I_p$  versus  $f^{1/2}$ .

**Table 1.** Half-peak width and transfer electron number of Yb(III) calculated on a liquid Pb electrode in molten LiCl-KCl-YbCl<sub>3</sub> under different frequencies.

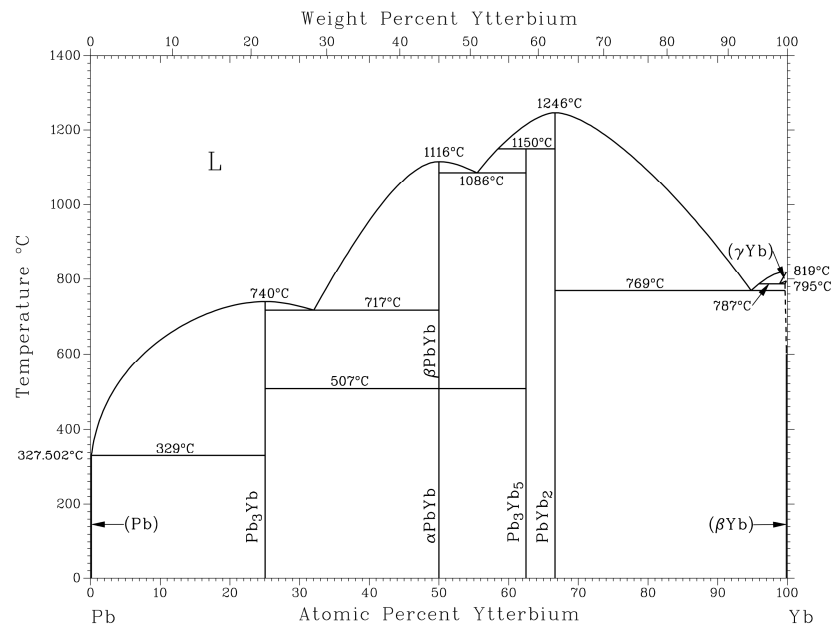
| $f/\text{Hz}$ | $W_{1/2}/\text{V}$ | $n$   |
|---------------|--------------------|-------|
| 5             | 0.259              | 0.907 |
| 10            | 0.251              | 0.934 |
| 15            | 0.251              | 0.934 |
| 20            | 0.243              | 0.963 |
| 30            | 0.243              | 0.963 |
| 40            | 0.243              | 0.963 |

### 3.2. Electrochemical Properties of YbCl<sub>3</sub> on a Pb Film Electrode

The Pb film was prepared on the surface of the W electrode through PE at  $-1.0$  V for 1 s. Figure 6 shows the CVs on the W electrode before and after adding YbCl<sub>3</sub> and PbCl<sub>2</sub> to LiCl KCl molten salt. The peaks R<sub>B</sub> and R<sub>C</sub> in the inset of Figure 6 are related to the reduction of Pb(II) to Pb and Yb(III) to Yb(II), respectively. Based on the binary phase diagram of the Pb-Yb system [47] shown in Figure 7, there are four intermetallics (Pb<sub>3</sub>Yb, PbYb, Pb<sub>3</sub>Yb<sub>5</sub>, and PbYb<sub>2</sub>) in the study temperature range. Therefore, four reduction peaks (R<sub>I</sub>, R<sub>II</sub>, R<sub>III</sub>, and R<sub>IV</sub>) in the inset of Figure 6 correspond to four different Pb-Yb intermetallics. Pb(II) is first deposited on the W electrode to form a Pb film electrode. Then, Yb(II) is reduced at the corrected potential on the Pb film electrode due to depolarization to form Pb-Yb intermetallics. The reaction is as follows:

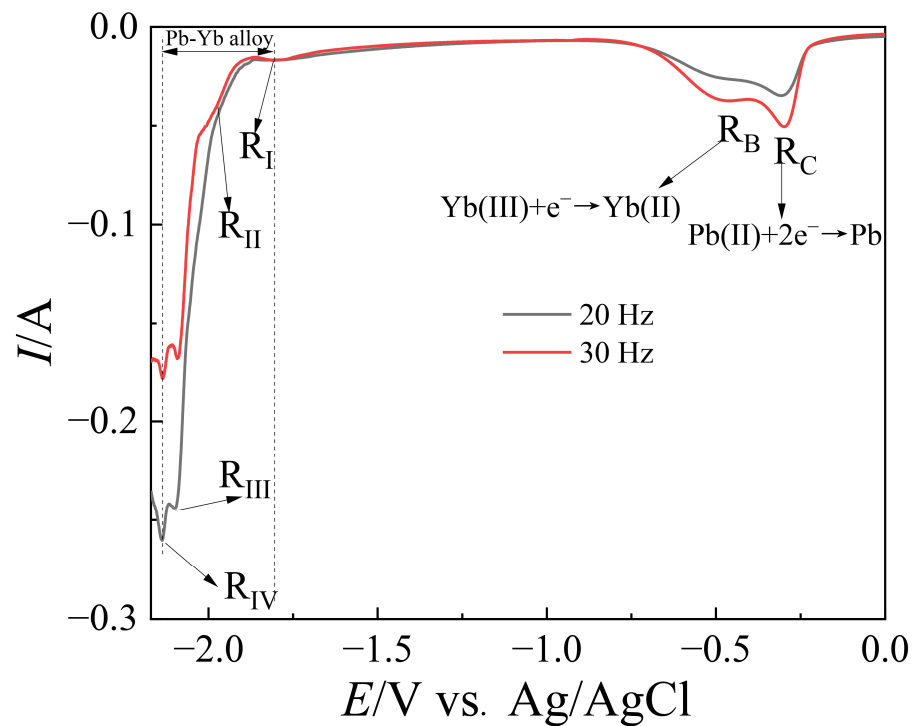


**Figure 6.** CVs of blank eutectic LiCl-KCl (black line) and molten LiCl-KCl-YbCl<sub>3</sub>-PbCl<sub>2</sub> salts (red line) on the W electrode at 773 K.



**Figure 7.** The binary phase diagram of the Pb-Yb system.

To confirm the attribution of the peaks, Figure 8 shows the SWV curves at different frequencies on the W electrode in molten LiCl-KCl-YbCl<sub>3</sub>-PbCl<sub>2</sub>. Six reductive peaks were observed clearly in Figure 8. Two reduction signals R<sub>B</sub> and R<sub>C</sub> pertain to the reduction of Yb(III) to Yb(II) and Pb(II) to Pb, respectively. Four reduction peaks R<sub>I</sub>, R<sub>II</sub>, R<sub>III</sub>, and R<sub>IV</sub> are associated with four Pb-Yb intermetallics. The reduction peak potentials are listed in Table 2.

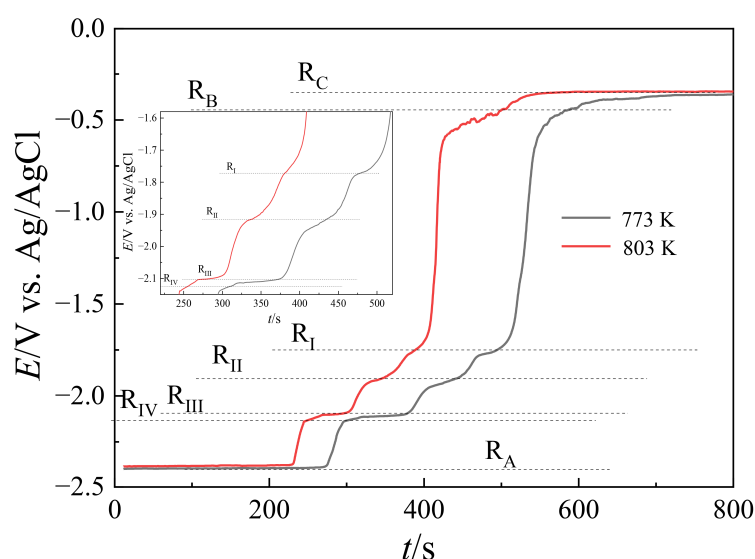


**Figure 8.** SWV curves of molten LiCl-KCl-YbCl<sub>3</sub>-PbCl<sub>2</sub> on the W electrode at 773 K under different frequencies; potential step: 5 mV; frequency: 20–30 Hz.

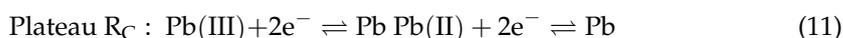
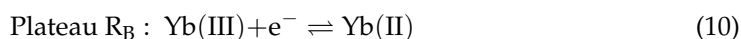
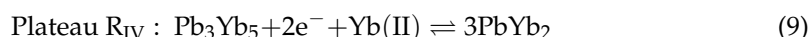
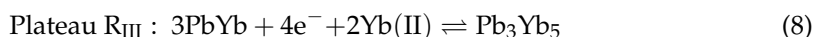
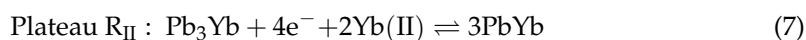
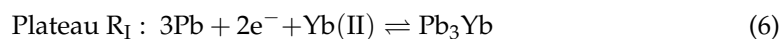
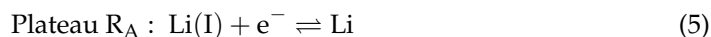
**Table 2.** Summary of the results obtained on a Pb film electrode through CV, SWV, and OCP in molten LiCl-KCl-YbCl<sub>3</sub>.

| Electrochemical Techniques | Reduction of Peak/Plateau Potentials |       |       |       |
|----------------------------|--------------------------------------|-------|-------|-------|
|                            | IV                                   | III   | II    | I     |
| CV (V)                     | −2.15                                | −2.10 | −1.95 | −1.79 |
| SWV (V)                    | −2.13                                | −2.09 | −1.96 | −1.80 |
| OCP (V)                    | −2.12                                | −2.09 | −1.92 | −1.77 |

To explore the electroextraction of Yb, open circuit chronopotentiometry (OCP) was used in LiCl-KCl-YbCl<sub>3</sub>-PbCl<sub>2</sub> melts at various temperatures. Figure 9 displays the OCP curves measured on the Pb film electrode after deposition at −2.5 V for 100 s in molten LiCl-KCl-YbCl<sub>3</sub>-PbCl<sub>2</sub> at 773–833 K.

**Figure 9.** OCP curves recorded on the W electrode in molten LiCl-KCl-YbCl<sub>3</sub>-PbCl<sub>2</sub>; deposition potential: −2.5 V; time: 100 s.

Plateau R<sub>B</sub> and R<sub>C</sub> were observed at −0.43 V and −0.33 V and were assigned to Yb(III)/Yb(II) and Pb(II)/Pb(0) redox couples, respectively. The four plateaus R<sub>I</sub>, R<sub>II</sub>, R<sub>III</sub>, and R<sub>IV</sub> were correlated to the equilibrium of Pb-Yb intermetallics. We speculated that the potential plateaus should be related to the following equilibriums:



### 3.3. Electrochemical Property of Yb(III) Ions on the Liquid Pb Electrode

Figure 10 is the cyclic voltammogram of LiCl-KCl-YbCl<sub>3</sub> molten salt on a liquid Pb electrode. Signal C relates to the reduction of Pb(II) to Pb, and signal R<sub>B</sub> relates to the reduction of Yb(III) to Yb(II). The conclusion is consistent with that discussed above. This indicates that Yb(III) is first reduced to Yb(II) on the liquid Pb electrode, and then Yb(II) is

reduced to Yb. One signal that appears at  $-1.71$  V corresponds to the formation of a solid Yb(Pb) solution.

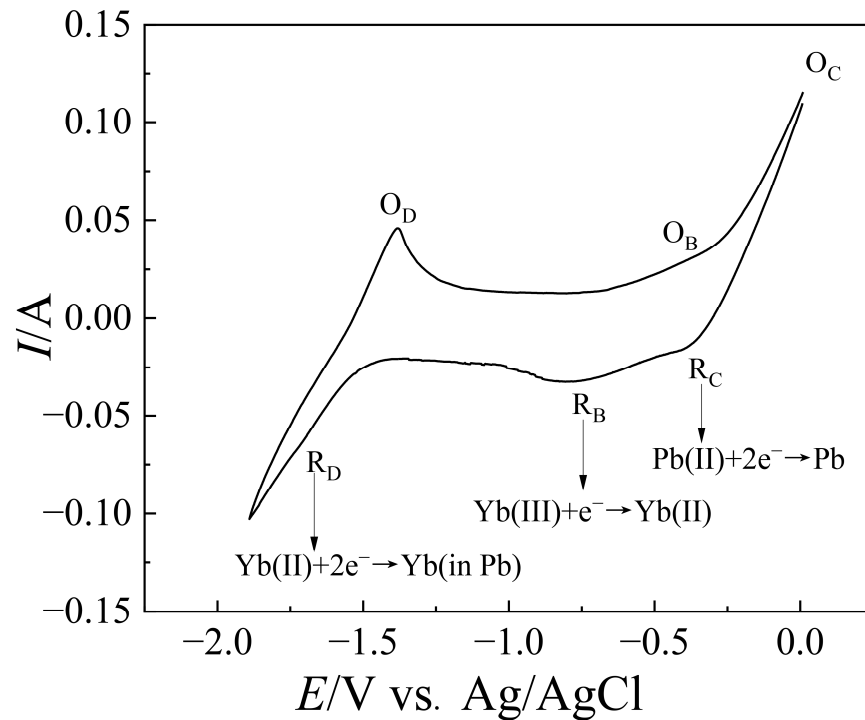


**Figure 10.** CVs obtained in LiCl-KCl-YbCl<sub>3</sub> ( $1.55 \times 10^{-4}$  mol cm<sup>-3</sup>) melt on liquid Pb cathodes ( $S = 0.949$  cm<sup>2</sup>) at 773 K.

According to the CV results above, Yb was extracted by PE at  $-1.86$  V on a liquid Pb electrode. Figure 11 shows the alloy's XRD pattern obtained by electrolysis at constant potential  $-1.86$  V for 6, 10, and 14 h, respectively, on the liquid Pb electrode in molten LiCl-KCl-YbCl<sub>3</sub> at 773 K. The alloy electrolyzed for 6 h was the Pb<sub>3</sub>Yb phase, the alloy electrolyzed for 10 h was the Pb<sub>3</sub>Yb phase, and the alloys electrolyzed for 14 h were Pb<sub>3</sub>Yb and PbYb phases. This shows that with the increase of electrolysis time, the content of Yb in liquid lead gradually increased, and part of Pb<sub>3</sub>Yb began to transform into the PbYb phase.

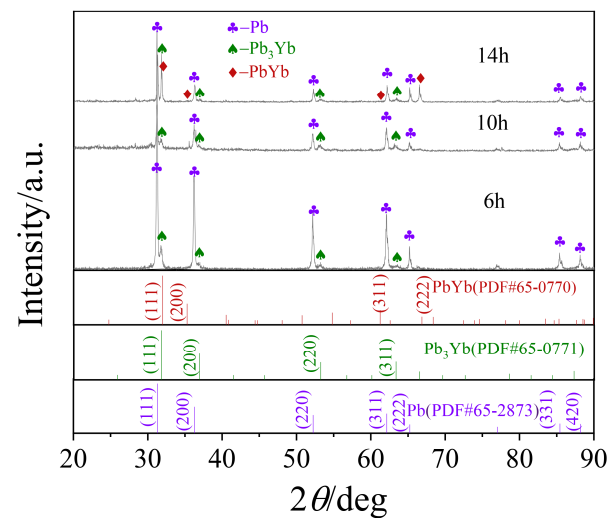


**Figure 11.** XRD patterns of the cathode products on a liquid Pb electrode in molten LiCl-KCl-YbCl<sub>3</sub> salts through PE at  $-1.86$  V for 14 h at 773 K.

After electrolysis for 14 h, the alloy was analyzed by SEM-EDS, and the SEM photograph and element distribution surface scan of the alloy were obtained, as shown in Figure 12. Two zones, dark and bright grey, were on the deposit's surface. From the results of the EDS mapping of the sample (Figure 12b), the element Yb mainly distributed in the dark grey zone. The upper salt was detected by inductively coupled plasma atomic emission spectrometry (ICP-AES). It was calculated that after electrolytic extraction for 14 h, the extraction rate of Yb was 94.5%.

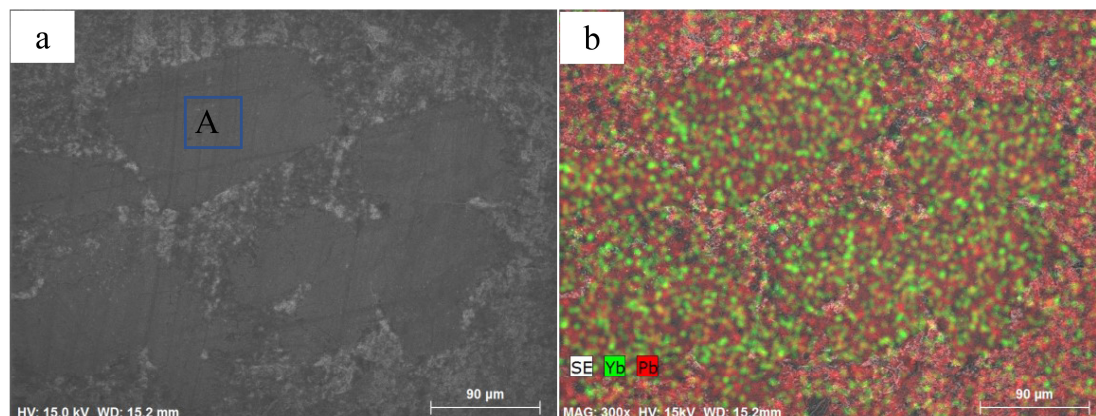


**Figure 12.** SEM image (a) and EDS mapping (b) analysis of the deposit obtained by PE at  $-1.86$  V on a liquid Pb electrode in molten LiCl-KCl-YbCl<sub>3</sub> salts for 14 h at 773 K.

#### 4. Conclusions

In this work, the electroreduction of Yb(III) ions on the W cathode was explored through CV and SWV. The electroreduction of Yb(III) to Yb(II) was found to be a diffusion-controlled process with one electron exchanged, and the reduction of Yb(III)/Yb(II) was a reversible process. The diffusion coefficient of Yb(III) was  $1.86 \times 10^{-5} \text{ cm}^2 \text{ s}^{-1}$ . The electrochemical behavior of Yb(III) on a liquid Pb film cathode was explored by CV, SWV, and OCP. Then, equilibrium potentials and the deposition potentials of four Pb-Yb intermetallics (Pb<sub>3</sub>Yb, PbYb, Pb<sub>3</sub>Yb<sub>5</sub>, and PbYb<sub>2</sub>) were determined. The reduction of Yb(III) on liquid Pb and liquid Pb film electrodes was proven to be a two-step mechanism.

At last, the electrochemical extraction of Yb(III) on a liquid Pb electrode was studied by CV. Meanwhile, ytterbium was extracted on a liquid Pb electrode from a LiCl-KCl melt by PE at  $-1.86$  V. The extraction product was detected by SEM-EDS and XRD. XRD analysis of the extracted products obtained at different electrolysis times shows that the extracted products gradually changed from a Pb-rich alloy (Pb<sub>3</sub>Yb) to a Yb-rich alloy (Pb<sub>3</sub>Yb and PbYb) with the increase in electrolysis extraction time. The extraction efficiency of Yb reached up to 94.5% by PE at  $-1.86$  V for 14 h, which indicates that it is feasible to electrolytically extract Yb from LiCl-KCl melts on a liquid Pb electrode.

**Author Contributions:** Conceptualization, Investigation, Writing—original draft, Z.L. (Zhuyao Li); Investigation, Software, L.Z. (Liandi Zhu); Methodology, Resources, D.T. Supervision, Y.D.; Formal analysis, Investigation, F.H. and Z.G.; Data curation, C.L. and H.L.; Supervision, L.Z. (Limin Zhou) and Z.L. (Zhirong Liu); Project administration, J.O. All authors have read and agreed to the published version of the manuscript.

**Funding:** The paper was financially co-supported by the National Natural Science Foundation of China (11905029, 22176032, and 11875105) and the Independent fund of State Key Laboratory of Nuclear Resources and Environment of East China University of Technology (2020Z19). Academic and technical leader training program for major disciplines in Jiangxi Province (20212BCJ23001).

**Conflicts of Interest:** The authors declare no conflict of interest.

## References

1. Karley, D.; Shukla, S.K.; Rao, T.S. Microbiological assessment of spent nuclear fuel pools: An in-perspective review. *J. Environ. Chem. Eng.* **2022**, *10*, 108050. [[CrossRef](#)]
2. Grebennikova, T.; Jones, A.N.; Sharrad, C.A. Electrochemical decontamination of irradiated nuclear graphite from corrosion and fission products using molten salt. *Energ. Environ. Sci.* **2021**, *14*, 5501–5512. [[CrossRef](#)]
3. Du, Y.; Tang, H.; Zhang, D.; Shao, L.; Li, Y.; Gao, R.; Yang, Z.; Li, B.; Chu, M.; Liao, J. Electro-reduction processes of  $U_3O_8$  to metallic U bulk in LiCl molten salt. *J. Nucl. Mater.* **2021**, *543*, 152627. [[CrossRef](#)]
4. Lichtenstein, T.; Nigl, T.P.; Smith, N.D.; Kim, H. Electrochemical deposition of alkaline-earth elements (Sr and Ba) from LiCl-KCl-SrCl<sub>2</sub>-BaCl<sub>2</sub> solution using a liquid bismuth electrode. *Electrochim. Acta* **2018**, *281*, 810–815. [[CrossRef](#)]
5. Kurniawan, T.A.; Othman, M.H.D.; Singh, D.; Avtar, R.; Hwang, G.H.; Setiadi, T.; Lo, W.H. Technological solutions for long-term storage of partially used nuclear waste: A critical review. *Ann. Nucl. Energy* **2022**, *166*, 108736. [[CrossRef](#)]
6. Zohuri, B. Nuclear Fuel Cycle and Decommissioning. In *Nuclear Reactor Technology Development and Utilization*; Elsevier: Amsterdam, The Netherlands, 2020; pp. 61–120.
7. Taylor, R.; Bodel, W.; Stamford, L.; Butler, G. A Review of Environmental and Economic Implications of Closing the Nuclear Fuel Cycle—Part One: Wastes and Environmental Impacts. *Energies* **2022**, *15*, 1433. [[CrossRef](#)]
8. Burek, J.; Nutter, D. Life cycle assessment of grocery, perishable, and general merchandise multi-facility distribution center networks. *Energy Build.* **2018**, *174*, 388–401. [[CrossRef](#)]
9. Zhong, Y.K.; Liu, Y.L.; Liu, K.; Wang, L.; Mei, L.; Gibson, J.K.; Chen, J.Z.; Jiang, S.L.; Liu, Y.C.; Yuan, L.Y. In-situ anodic precipitation process for highly efficient separation of aluminum alloys. *Nat. Commun.* **2021**, *12*, 1–6. [[CrossRef](#)]
10. Zhang, Y.; Song, J.; Li, X.; Yan, L.; Shi, S.; Jiang, T.; Peng, S. First principles calculation of redox potential for tetravalent actinides in molten LiCl-KCl eutectic based on vertical substitution and relaxation. *Electrochim. Acta* **2019**, *293*, 466–475. [[CrossRef](#)]
11. Wang, Y.; Quan, M.; Zhang, S.; Liu, Y.; Wang, Y.; Dai, Y.; Dong, Z.; Cheng, Z.; Zhang, Z.; Liu, Y. Electrochemical extraction of gadolinium on Sn electrode and preparation of Sn-Gd intermetallic compounds in LiCl-KCl melts. *J. Alloy. Compd.* **2022**, *907*, 164220. [[CrossRef](#)]
12. Han, W.; Li, Z.; Li, M.; Li, W.; Zhang, M.; Yang, X.; Sun, Y. Reductive extraction of lanthanides (Ce, Sm) and its monitoring in LiCl-KCl/Bi-Li system. *J. Nucl. Mater.* **2019**, *514*, 311–320. [[CrossRef](#)]
13. Im, S.; Smith, N.D.; Baldvieso, S.C.; Gesualdi, J.; Liu, Z.K.; Kim, H. Electrochemical recovery of Nd using liquid metals (Bi and Sn) in LiCl-KCl-NdCl<sub>3</sub>. *Electrochim. Acta* **2022**, *425*, 140655. [[CrossRef](#)]
14. Williamson, M.; Willit, J. Pyroprocessing flowsheets for recycling used nuclear fuel. *Nucl. Eng. Technol.* **2011**, *43*, 329–334. [[CrossRef](#)]
15. Liu, K.; Chai, Z.F.; Shi, W.Q. Liquid Electrodes for An/Ln Separation in Pyroprocessing. *J. Electrochem. Soc.* **2021**, *168*, 032507. [[CrossRef](#)]
16. Solbrig, C.; Westphal, B.; Johnson, T.; Li, S.; Marsden, K.; Goff, K. *Pyroprocessing Progress at Idaho National Laboratory*; Idaho National Lab. (INL): Idaho Falls, ID, USA, 2007.
17. Wang, D.D.; Liu, Y.L.; Yang, D.W.; Zhong, Y.K.; Han, W.; Wang, L.; Chai, Z.F.; Shi, W.Q. Separation of uranium from lanthanides (La, Sm) with sacrificial Li anode in LiCl-KCl eutectic salt. *Sep. Purif. Technol.* **2022**, *292*, 121025. [[CrossRef](#)]
18. Han, W.; Li, Z.; Li, M.; Li, W.; Zhang, X.; Yang, X.; Zhang, M.; Sun, Y. Electrochemical extraction of holmium and thermodynamic properties of Ho-Bi alloys in LiCl-KCl eutectic. *J. Electrochem. Soc.* **2017**, *164*, E62. [[CrossRef](#)]
19. Han, W.; Li, Z.; Li, M.; Hu, X.; Yang, X.; Zhang, M.; Sun, Y. Electrochemical behavior and extraction of holmium on Cu electrode in LiCl-KCl molten salt. *J. Electrochem. Soc.* **2017**, *164*, D934. [[CrossRef](#)]
20. Jiang, S.; Lan, J.; Wang, L.; Liu, Y.; Zhong, Y.; Liu, Y.; Yuan, L.L.Y.; Zheng, L.; Chai, Z.; Shi, W. Competitive Coordination of Chloride and Fluoride Anions Towards Trivalent Lanthanide Cations (La<sup>3+</sup> and Nd<sup>3+</sup>) in Molten Salts. *Chem. Eur. J.* **2021**, *27*, 11721–11729. [[CrossRef](#)] [[PubMed](#)]
21. Jiang, S.; Liu, Y.; Wang, L.; Chai, Z.; Shi, W.Q. The Coordination Chemistry of f-Block Elements in Molten Salts. *Chem. Eur. J.* **2022**, e202201145. [[CrossRef](#)] [[PubMed](#)]
22. Liu, Y.; Liu, Y.; Wang, L.; Jiang, S.; Zhong, Y.; Wu, Y.; Li, M.; Shi, W. Chemical Species Transformation during the Dissolution Process of  $U_3O_8$  and  $UO_3$  in the LiCl-KCl-AlCl<sub>3</sub> Molten Salt. *Inorg. Chem.* **2022**, *61*, 6519–6529. [[CrossRef](#)]
23. Liu, Y.C.; Liu, Y.L.; Zhao, Y.; Liu, Z.; Zhou, T.; Zou, Q.; Zeng, X.; Zhong, Y.K.; Li, M.; Sun, Z.X. A simple and effective separation of  $UO_2$  and  $Ln_2O_3$  assisted by  $NH_4Cl$  in LiCl-KCl eutectic. *J. Nucl. Mater.* **2020**, *532*, 152049. [[CrossRef](#)]
24. Jiao, S.Q.; Jiao, H.D.; Song, W.L.; Wang, M.Y.; Tu, J.G. A review on liquid metals as cathodes for molten salt/oxide electrolysis. *Int. J. Min. Met. Mater.* **2020**, *27*, 1588–1598. [[CrossRef](#)]
25. Yang, D.W.; Jiang, S.L.; Liu, Y.L.; Geng, J.S.; Li, M.; Wang, L.; Chai, Z.F.; Shi, W.Q. Electrochemical extraction kinetics of Nd on reactive electrodes. *Sep. Purif. Technol.* **2022**, *281*, 119853. [[CrossRef](#)]
26. Yin, T.; Liu, Y.; Yang, D.; Yan, Y.; Wang, G.; Chai, Z.; Shi, W. Thermodynamics and kinetics properties of lanthanides (La, Ce, Pr, Nd) on liquid bismuth electrode in LiCl-KCl molten salt. *J. Electrochem. Soc.* **2020**, *167*, 122507. [[CrossRef](#)]
27. Yin, T.; Liu, Y.; Jiang, S.; Yan, Y.; Wang, G.; Chai, Z.; Shi, W. Kinetic Properties and Electrochemical Separation of Uranium on Liquid Bismuth Electrode in LiCl-KCl Melt. *J. Electrochem. Soc.* **2021**, *168*, 032503. [[CrossRef](#)]
28. Jiang, S.; Liu, K.; Liu, Y.; Yin, T.; Chai, Z.; Shi, W. Electrochemical behavior of Th (IV) on the bismuth electrode in LiCl-KCl eutectic. *J. Nucl. Mater.* **2019**, *523*, 268–275. [[CrossRef](#)]

29. Han, W.; Li, W.; Chen, J.; Li, M.; Li, Z.; Dong, Y.; Zhang, M. Electrochemical properties of yttrium on W and Pb electrodes in LiCl–KCl eutectic melts. *RSC Adv.* **2019**, *9*, 26718–26728. [[CrossRef](#)] [[PubMed](#)]
30. Li, M.; Sun, Z.; Guo, D.; Han, W.; Sun, Y.; Yang, X.; Zhang, M. Electrode reaction of Pr (III) and coreduction of Pr (III) and Pb (II) on W electrode in eutectic LiCl–KCl. *Ionics* **2020**, *26*, 3901–3909. [[CrossRef](#)]
31. Han, W.; Wang, W.; Li, M.; Wang, D.; Li, H.; Chen, J.; Sun, Y. Electrochemical separation of La from LiCl–KCl fused salt by forming La–Pb alloys. *Sep. Purif. Technol.* **2021**, *275*, 119188. [[CrossRef](#)]
32. Han, W.; Wang, W.; Li, M.; Meng, Y.; Ji, W.; Sun, Y. Electrochemical coreduction of Gd (III) with Pb (II) and recovery of Gd from LiCl–KCl eutectic assisted by Pb metal. *J. Electrochem. Soc.* **2020**, *167*, 142505. [[CrossRef](#)]
33. Han, W.; Wang, W.; Li, M.; Wang, J.; Sun, Y.; Yang, X.; Zhang, M. Electrochemical behavior and extraction of zirconium on Sn-coated W electrode in LiCl–KCl melts. *Sep. Purif. Technol.* **2020**, *232*, 115965. [[CrossRef](#)]
34. Sun, C.; Xu, Q.; Yang, Y.; Zou, X.; Cheng, H.; Lu, X. Effect of the Li Reduction to Electrodeposition of Nd–Sn Compounds in Liquid Sn Electrode in LiCl–KCl–NdCl<sub>3</sub> Melt. *J. Electrochem. Soc.* **2021**, *168*, 102505. [[CrossRef](#)]
35. Han, W.; Wang, W.; Zhang, Y.; Wang, Y.; Li, M.; Sun, Y. Electrode reaction of Pr on Sn electrode and its electrochemical recovery from LiCl–KCl molten salt. *Int. J. Energ. Res.* **2021**, *45*, 8577–8592. [[CrossRef](#)]
36. Li, M.; Sun, Z.; Han, W.; Sun, Y.; Yang, X.; Wang, W. Electrochemical reaction of Sm (III) on liquid Sn electrode. *J. Electrochem. Soc.* **2020**, *167*, 022502. [[CrossRef](#)]
37. Liu, K.; Liu, Y.L.; Chai, Z.F.; Shi, W.Q. Evaluation of the electroextractions of Ce and Nd from LiCl–KCl molten salt using liquid Ga electrode. *J. Electrochem. Soc.* **2017**, *164*, D169. [[CrossRef](#)]
38. Yang, D.W.; Jiang, S.L.; Liu, Y.L.; Yin, T.Q.; Li, M.; Wang, L.; Luo, W.; Chai, Z.F.; Shi, W.Q. Electrodeposition Mechanism of La<sup>3+</sup> on Al, Ga and Al–Ga Alloy Cathodes in LiCl–KCl Eutectic Salt. *J. Electrochem. Soc.* **2021**, *168*, 062511. [[CrossRef](#)]
39. Yang, D.W.; Liu, Y.L.; Yin, T.Q.; Li, M.; Han, W.; Chang, K.-K.; Chai, Z.-F.; Shi, W.Q. Co-reduction behaviors of Ce (III), Al (III) and Ga (III) on a W electrode: An exploration for liquid binary Al–Ga cathode. *Electrochim. Acta* **2019**, *319*, 869–877. [[CrossRef](#)]
40. Yang, D.W.; Liu, Y.L.; Yin, T.Q.; Jiang, S.L.; Zhong, Y.K.; Wang, L.; Li, M.; Chai, Z.F.; Shi, W.Q. Application of binary Ga–Al alloy cathode in U separation from Ce: The possibility in pyroprocessing of spent nuclear fuel. *Electrochim. Acta* **2020**, *353*, 136449. [[CrossRef](#)]
41. Li, Z.; Liu, Z.; Li, W.; Han, W.; Li, M.; Zhang, M. Electrochemical recovery of dysprosium from LiCl–KCl melt aided by liquid Pb metal. *Sep. Purif. Technol.* **2020**, *250*, 117124. [[CrossRef](#)]
42. Li, Z.; Tang, D.; Meng, S.; Gu, L.; Dai, Y.; Liu, Z. Electrolytic separation of Dy from Sm in molten LiCl–KCl using Pb–Bi eutectic alloy cathode. *Sep. Purif. Technol.* **2021**, *276*, 119045. [[CrossRef](#)]
43. Wang, P.; Han, W. Electrochemical and thermodynamic properties of ytterbium and formation of Zn–Yb alloy on liquid Zn electrode. *J. Nucl. Mater.* **2019**, *517*, 157–164. [[CrossRef](#)]
44. Li, M.; Liu, B.; Ji, N.; Sun, Y.; Han, W.; Jiang, T.; Peng, S.; Yan, Y.; Zhang, M. Electrochemical extracting variable valence ytterbium from LiCl–KCl–YbCl<sub>3</sub> melt on Cu electrode. *Electrochim. Acta* **2016**, *193*, 54–62. [[CrossRef](#)]
45. Zheng, J.; Yin, T.; Wang, P.; Yan, Y.; Smolenski, V.; Novoselova, A.; Zhang, M.; Ma, F.; Xue, Y. Electrochemical extraction of ytterbium from LiCl–KCl–YbCl<sub>3</sub>–ZnCl<sub>2</sub> melt by forming Zn–Yb alloys. *J. Solid State Electrochem.* **2022**, *26*, 1067–1074. [[CrossRef](#)]
46. Smolenski, V.; Novoselova, A.; Osipenko, A.; Caravaca, C.; De Córdoba, G. Electrochemistry of ytterbium (III) in molten alkali metal chlorides. *Electrochim. Acta* **2008**, *54*, 382–387. [[CrossRef](#)]
47. Palenzona, A.; Cirafici, S. The Pb–Yb (Lead–Ytterbium) system. *J. Phase Equilib. Diff.* **1991**, *12*, 479–481. [[CrossRef](#)]